Eur. Phys. J. Special Topics **226**, 1811–1828 (2017)

DOI: 10.1140/epjst/e2016-60396-5

THE EUROPEAN PHYSICAL JOURNAL SPECIAL TOPICS

Regular Article

Electronic circuit analog of synthetic genetic networks: Revisited

Edward H. Hellen[1,a], Jürgen Kurths[2], and Syamal K. Dana[3]

[1] Department of Physics and Astronomy, University of North Carolina Greensboro, Greensboro, NC 27402, USA
[2] Potsdam Institute for Climate Impact Research, Potsdam, Germany
[3] Department of Mathematics, Jadavpur University, Kolkata 700032, India

Received 20 December 2016 / Received in final form 2 March 2017
Published online 21 June 2017

Abstract. Electronic circuits are useful tools for studying potential dynamical behaviors of synthetic genetic networks. The circuit models are complementary to numerical simulations of the networks, especially providing a framework for verification of dynamical behaviors in the presence of intrinsic and extrinsic noise of the electrical systems. Here we present an improved version of our previous design of an electronic analog of genetic networks that includes the 3-gene Repressilator and we show conversions between model parameters and real circuit component values to mimic the numerical results in experiments. Important features of the circuit design include the incorporation of chemical kinetics representing Hill function inhibition, quorum sensing coupling, and additive noise. Especially, we make a circuit design for a systematic change of initial conditions in experiment, which is critically important for studies of dynamical systems' behavior, particularly, when it shows multistability. This improved electronic analog of the synthetic genetic network allows us to extend our investigations from an isolated Repressilator to coupled Repressilators and to reveal the dynamical behavior's complexity.

1 Introduction

Synthetic genetic networks (SGN) provide a potential tool to design useful biologically based circuitry targeted to perform specific tasks [1–3]. In principle, such circuits can be incorporated into natural cellular machinery or used in an entirely synthetic environment. The early stages of research in this direction were to envision and understand simple networks which provided the basic components for building more complex functional devices. Emphasis was first given to the design of a genetic toggle switch [4] and an oscillator known as the Repressilator consisting of a 3-gene inhibitory ring that has been expressed in *E. coli* [5]. Later, electronic circuits were suggested and used to study the dynamics of synthetic genetic networks [6–9]. Electronic circuits, in general, allow precise control of system parameters and provide

[a] e-mail: ehhellen@uncg.edu

a minimal set-up for experimenting with a dynamical behavior in the presence of intrinsic and extrinsic noises. This option is useful, to predict various desired functional behaviors in electronic analogs of synthetic genetic networks which are difficult to control in real biological experiments.

We have designed electronic circuits, in the past, to model genetic networks configured to investigate dynamical behaviors of the Repressilator [10,11] and to perform noise-aided logic operations [12]. In the Repressilator studies, we first considered an isolated Repressilator and verified the functional form of the predicted oscillations [10]. Then we incorporated a bacterial-inspired method of quorum sensing (QS) coupling [13] into our Repressilator circuit by adding a feedback chain to the 3-gene inhibitory ring. This additional pathway led to a rich variety of dynamical behavior, including multistability, for the QS-modified isolated Repressilator [11]. Simulations of this single Repressilator system have even demonstrated period doubling chaotization [14]. The next step of allowing the QS mechanism to couple Repressilators together as has been done in simulation [13,15,16] proved difficult using our previous circuit models. This difficulty lead us to make improvements of the circuit including a complete redesign of the QS circuitry, which we present here in detail. The improved design allowed us to investigate the more complex dynamics that exist for coupled Repressilators [17] and to access the full QS-parameter range of the mathematical model. Apart from their potential use in synthetic biological devices, coupled Repressilators are of interest because they belong to the field of coupled nonlinear oscillators which is essential for the understanding of a wide variety of biological phenomena [18].

For two QS-coupled repressilators using "repressive" coupling [15], the improved circuit demonstrates a variety of states: homogeneous and inhomogeneous steady-states, homogeneous and inhomogeneous limit cycles, and a rich variety of complex oscillations heavily influenced by the existence of asymmetric and symmetric high-period limit cycles [17]. The dominant homogeneous limit cycle is an anti-phase oscillation (180° between the two repressilator oscillations) which exists over a broad range of coupling strength. In-phase limit cycle exists only in a narrow parameter range. In the range of coupling strength where torus bifurcation makes the anti-phase LC unstable, it is replaced by a rich variety of complex dynamics and stable symmetric and asymmetric high period limit cycles. Multi-stability is found over broad ranges of coupling strength in both the stable and unstable regions of the anti-phase limit cycle.

It is crucial to have a precise control of the initial conditions when studying a multistable system like the QS-coupled Repressilators so that all of the coexisting attractors for a given set of parameters can be captured. We describe the use of an analog switch to set the initial conditions by initializing capacitor voltages to the desired values. Multistability also opens the possibility of noise-induced transitions from one attractor to another. Therefore we use our previous noise circuit [12] and the genetic network circuit as a test-bed to demonstrate noise-induced transitions between attractors within the QS-coupled Repressilator system. We begin with the mathematical model and the analog circuit for the genetic network of Repressilators coupled via QS. Then we present our circuit analysis which relates the circuit to the mathematical model. Next, we use the QS circuit to verify the numerical predictions, and we show results for QS-coupled Repressilator circuits. Finally, we describe how to set the initial conditions and incorporate additive noise in the electronic circuit.

2 Model: repressilator with quorum sensing

We present here the mathematical model and the circuit model for the genetic network of our interest. The following sections show our analysis which connects the circuits to the equations.

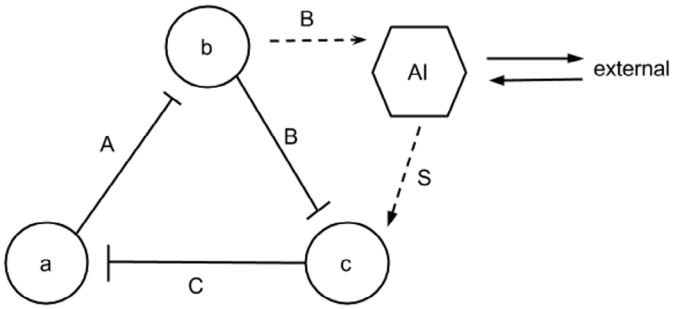

Fig. 1. Repressilator with quorum sensing feedback. Genes indicated by their transcribed mRNA (a, b, c), and their expressed proteins (A, B, C) form the 3-gene inhibitory loop referred to as the Repressilator. Quorum sensing is provided by the additional feedback loop of the small auto-inducer molecule which can diffuse through the cell membrane thereby exchanging with the external medium. In this way gene-b has competing roles of direct inhibition and indirect activation of gene-c. S is the concentration of the auto-inducer.

Figure 1 shows a Repressilator with a QS feedback loop. Genes expressing mRNA (a, b, c) and their expressed proteins (A, B, C) form the 3-gene inhibitory loop referred to as the Repressilator [5]. It is named Repressilator because each gene's output "represses" the next gene's expression, resulting in stable oscillations of protein concentrations over a very broad interval of parameter values. Thus the Repressilator works as a genetic oscillator and is an example of a "ring oscillator" which consists of an odd number of inverters connected in a closed loop. It is a small network comprised of only three genes. Coupling Repressilators together creates a larger genetic network with possibilities of interesting and useful collective behaviors.

A natural choice for the coupling mechanism is bacterial QS in which each Repressilator contributes to, and responds to, a shared pool of a "signal" molecule [19]. The QS feedback loop uses a small auto-inducer (AI) molecule to provide an indirect activation path from B to C to compete with the direct inhibition [16]. This network structure generally leads to an anti-phase synchronization of two coupled Repressilators, meaning there is a 180° phase difference between the protein oscillations of the two Repressilators. A different network structure placing the feedback loop from A to C has also been employed [13], which generally leads to in-phase synchrony. Interestingly, the network structure does not fully determine the type of synchronization observed between coupled Repressilators as both of these structures are birhythmic – capable of both types of synchrony – depending on the model's parameter values [20]. This birhythmic property may be of use in the design of task-oriented devices.

We use our reduced mathematical model for QS-coupled Repressilators [11] which is based on previous models [5,16] and applies to the case of fast mRNA kinetics compared to protein kinetics. The model uses standard chemical kinetics $(\beta, \alpha, \kappa, n, k_i)$ including Hill function inhibition, $1/(1+x^n)$, and is

$$\frac{dA}{dt} = \beta_1 \left(-A + \frac{\alpha}{1+C^n} \right) \tag{1a}$$

$$\frac{dB}{dt} = \beta_2 \left(-B + \frac{\alpha}{1+A^n} \right) \tag{1b}$$

$$\frac{dC}{dt} = \beta_3 \left(-C + \frac{\alpha}{1+B^n} + \frac{\kappa S}{1+S} \right) \tag{1c}$$

$$\frac{dS}{dt} = -k_{s0} S + k_{s1} B - \eta \left(S - S_{ext} \right). \tag{1d}$$

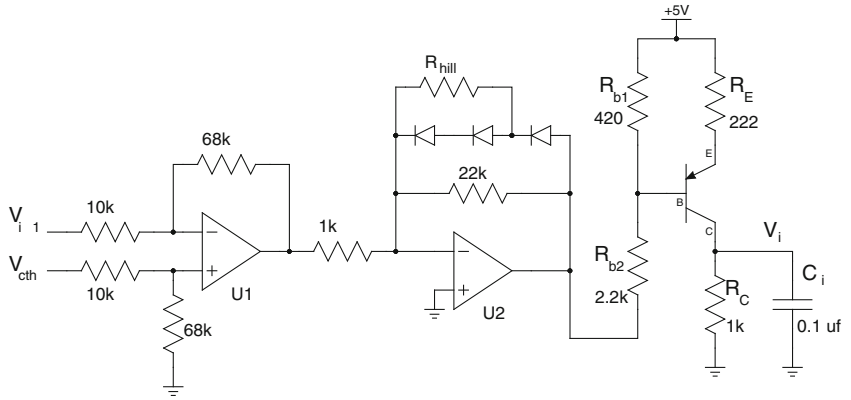

Fig. 2. Single-gene circuit. Inhibitory input at V_{i-1}. Expressed protein concentration is represented by V_i. Dual op-amp is LF412 supplied by ± 5 V. The *pnp* transistor is 2N3906. Resistor R_{hill} is adjusted to achieve desired Hill-function n value. Diodes are 1N4148. Capacitor value $C_i = 0.1\,\mu f$ is for $\beta = 1$. Reproduced from reference [17].

(A, B, C) are the protein concentrations for the Repressilator, and S is the concentration of the AI molecule. The AI can diffuse (diffusion constant η) through the cell membrane into the external medium, unlike the proteins which are confined inside the cell. S_{ext} is the AI concentration in the external medium and is a diluted average of the contributions from all the Repressilators, $S_{ext} = QS_{ave}$, where Q is the dilution factor. For results presented here we use $k_{s0} = 1$, $k_{s1} = 0.01$, and $\eta = 2$ as taken previously [16].

The circuit for a single inhibitory gene shown in Figure 2 is a modification of the previous one [10]. The transistor current represents the rate of gene expression and the voltage V_i represents the concentration of expressed protein. V_{i-1} represents the concentration of the inhibitor, and the V_{cth} adjusts the affinity of the inhibitor binding to the gene's DNA. The Hill function inhibition in equation (1) is accounted for by the dependence of the transistor current on inhibitor concentration voltage V_{i-1}. This dependence is derived in the next section.

The circuit for a Repressilator with quorum sensing feedback shown in Figure 3 is a complete redesign of that presented previously [11]. The Repressilator consists of the closed 3-gene loop with op-amp buffers between the genes. The QS circuitry takes input from current source $I(B)$ controlled by the repressilator's B-protein voltage, and feeds back to the Repressilator's C-protein via source I(S). The feedback activation in the mathematical model is through the binding-site occupation term $S/(1+S)$. We show below that the circuit accounts for the activation via QS by using a piece-wise continuous linear behavior, modeled by $\min(0.8S, 1)$ and hence we replace equation (1c) by

$$\frac{dC}{dt} = \beta_3 \left(-C + \frac{\alpha}{1 + B^n} + \kappa \, \min(0.8S, 1) \right). \tag{2}$$

In Figure 3, S_1 is the AI concentration belonging to the shown Repressilator. Coupling this Repressilator to a second Repressilator (not shown) is accomplished by adding their respective AI concentrations, S_1 and S_2, thus creating S_{ext}, the concentration of AI in the external medium. Figure 3 shows the connection of S_2 to the op-amp at the bottom of the figure and the combination with S_1 to produce S_{ext}.

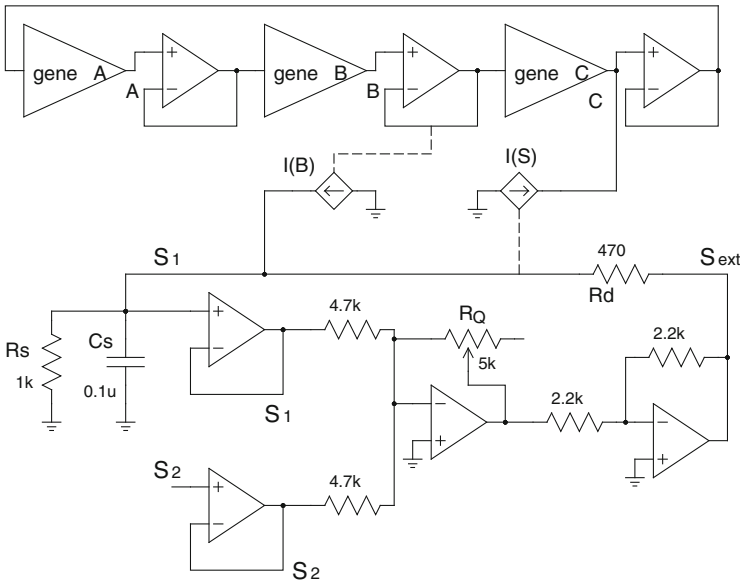

Fig. 3. Circuit for Repressilator with QS feedback. The Repressilator consists of the closed ring of genes A, B, and C. The quorum sensing loop is from B through S_1 to C. Protein B creates auto-inducer S_1 via the voltage-controlled current source $I(B)$, and S_1 activates production of C via $I(S)$. Each "gene" triangle corresponds to the single gene circuit in Figure 2. S_2 is the auto-inducer from a second Repressilator (not shown) and S_{ext} is the auto-inducer concentration in the external medium. R_Q sets the dilution factor, and R_d sets the diffusion rate through the membrane. Op-amps (LMC6062) powered by ± 5 V have low offset voltage (below 0.5 mV). Reproduced from reference [17].

2.1 Single gene circuit with Hill-function

We now analyse the circuit for a single gene and show how the inhibitory Hill function behavior is reproduced. In the process we find how to connect model parameters n and α to circuit parameters. We improve these connections over previous analyses [10,11] by incorporating the standard large-signal transistor model. In addition, we find the minimum accessible value of Hill coefficient n.

Applying current conservation to the capacitor voltage in Figure 2, and normalizing by a scaling parameter V_{th} gives,

$$R_C C_0 \frac{dx_i}{dt} = \frac{C_0}{C_i}\left(-x_i + \frac{I_t R_C}{V_{th}}\right) \tag{3}$$

where $x_i = V_i/V_{th}$ is the dimensionless protein concentration and I_t is the transistor's current collector. $R_C C_0$ is the time-scale which normalizes the time variable, thereby reassigning t to a dimensionless time. A comparison with equation (1) gives a useful relation between the model parameters and the circuit values,

$$\beta_i = \frac{C_0}{C_i}, \quad \alpha = \frac{I_{max} R_C}{V_{th}} \tag{4}$$

where I_{max} is the maximum transistor current. Its relation to I_t is defined below in the analysis of the circuit's modeling of the Hill function inhibition.

The gene inhibition in equation (1) is controlled by the Hill function

$$H(x) = \frac{1}{1 + x^n} \tag{5}$$

where x is the dimensionless inhibitory protein concentration. The scaling parameter V_{th} accounts for the inhibitor's equilibrium binding constant. Comparing equations (1) and (3) shows that the Hill function behavior must be accounted for in the circuit by the transistor current's dependence on input voltage V_{i-1}. In this section we derive this current-voltage dependence. The key elements are to get the correct slope at $x = 1$ where $H(x = 1) = 0.5$ and to approximate the Hill function's positive curvature as it decays to zero.

The op-amp U2 in Figure 2 has different gains, G_{-2} when $V_{i-1} < V_{cth}$, and G_{+2} when $V_{i-1} > V_{cth}$. For the selected component values in the circuit, the subtraction op-amp U1 has a gain $G_1 = -6.8$, and inverting op-amp U2 has $G_{-2} = -22$ and G_{+2} is an amplitude-dependent diminishing gain due to the three diodes in the feedback for U2. The diodes create the positive curvature decay of the Hill function.

The gene inhibition in the circuit corresponds to V_{i-1} surpassing V_{cth}, which causes the output of U2 to go positive and thereby turns off the *pnp* transistor resulting in no current from the collector. The maximum output voltage of U2 is about 2.0 V when the three diodes are fully conducting in their forward biased state. The resistors R_{b1} and R_{b2} are chosen such that an output voltage at U2 of 2.0 V causes a drop of $(0.42/2.62)(5 - 2) = 0.48$ V across R_{b1} which is small enough so that the transistor current is essentially zero. Maximal protein expression in the circuit corresponds to $V_{i-1} = 0$ which results in U2 output going negative with a limit at the lower saturation level $V_{-sat} = -3.5$ V for the dual op-amp LF412 supplied with ± 5 V. We assume that the gain $G_1 G_{-2}$ is large enough so that the output of U2 reaches V_{-sat} when $V_{i-1} = 0$. Later we determine a practical restriction on Hill coefficient n imposed by this assumption.

We predict the transistor's collector current in Figure 2 when the output of U2 varies between -3.5 and 2.0 V. The collector current is essentially the current in R_E since the transistor is in the active region. The voltage across R_{b1} is $s(5 - G\Delta V)$ where the fraction $s = 0.42/2.62 = 0.160$ is the voltage divider gain, $\Delta V = (V_{i-1} - V_{cth})$, and G is the overall gain of the 2 op-amps. The current in R_E, and therefore the transistor current, is

$$I_t = \frac{s(5 - G\Delta V) - V_{eb}}{R_E} \tag{6}$$

where V_{eb} is the emitter-base voltage. V_{eb} varies from about 0.5 V when there is essentially zero transistor current ($G\Delta V \approx 2$ V) to a maximum of about $V_{ebmx} = 0.70$ V at maximum current ($G\Delta V = V_{-sat}$). Maximal protein expression occurs for $V_{i-1} = 0$ (no inhibition) and thus $G\Delta V = V_{-sat}$ giving the maximum transistor current

$$I_{max} = \frac{s(5 - V_{-sat}) - V_{ebmx}}{R_E}. \tag{7}$$

For our chosen circuit components we measure $I_{max} = 2.95$ mA and $V_{ebmx} = 0.70$ V. This agrees well with the prediction using the large-signal transistor model with saturation current $I_S = 7$ fA (which we measured for the 2N3906 transistors), $V_{ebmx} = V_T \ln(I/I_S) = 0.026 \ln(2.95\,\text{mA}/7\,\text{fA}) = 0.696$ V. The resulting voltage drop across R_C is easily measured by setting $V_{i-1} = 0$, and agrees with that predicted by equation (7) flowing into $R_C = 1$ kΩ, $I_{max} R_C = 2.97$ V.

In the circuit, the Hill function equation (5) corresponds to the normalized transistor current

$$\frac{I_t}{I_{max}} = \frac{s(5 - G\Delta V) - V_{eb}}{s(5 - V_{-sat}) - V_{ebmx}}. \tag{8}$$

As presented previously [10], the circuit approximation of the Hill function is accomplished by setting the slope of the normalized current equal to the slope of the

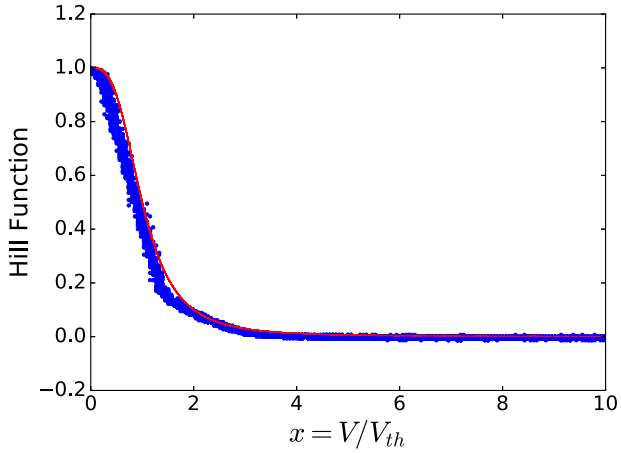

Fig. 4. Hill inhibition approximation for the single gene circuit in Figure 2. Numerical Hill inhibition (solid line) and experimentally measured (dots) normalized transistor current; $n = 3.2, \alpha = 218$, $R_{hill} = 4\,\mathrm{k}\Omega$. Data was collected with capacitor C_i removed. Reproduced from reference [17].

Hill function dH/dx at $x = 1$. Setting the slopes of equations (5) and (8) equal, using $\Delta V = V_{th}(x_{i-1} - V_{cth}/V_{th})$ with $x_{i-1} = 1$, gain $G = G_1 G_{-2}$, equation (7), and $V_{th} = I_{max} R_C/\alpha$ provides a useful result connecting important model parameters n and α to circuit parameters:

$$n\alpha = \frac{4sR_C G_1 G_{-2}}{R_E}. \tag{9}$$

Using our circuit values $s = 0.160$, $R_C = 1\,\mathrm{k}\Omega$, and $R_E = 222\,\Omega$, we determine $n\alpha = 2.88 G_1 G_{-2}$. Equation (9) allows desired model parameters n and α to be achieved in the circuit by adjusting gains G_1 and G_{-2}.

Next we find the relationship between the binding constant scaling voltage V_{th} and the circuit value V_{cth}. At $x = 1$ the Hill function has a value of 0.5. The corresponding condition for the circuit is that the normalized transistor current be 0.5 when $V_{i-1} = V_{th}$. By setting equation (8) equal to 0.5, letting $\Delta V = (V_{th} - V_{cth})$ and solving gives

$$V_{cth} = V_{th} + \frac{(2V_{eb} - V_{ebmx} - s\,(5 + V_{-sat}))}{2sG_1 G_{-2}}. \tag{10}$$

V_{eb} at half the maximal current is predicted by using 1.5 mA for the transistor current resulting in $V_{eb} = V_T \ln(I/I_S) = 0.026 \ln(1.5\,\mathrm{mA}/7\,\mathrm{fA}) = 0.678\,\mathrm{V}$. For the circuit in Figure 2, $G_1 G_{-2} = (-6.8)(-22)$, $s = 0.160$, $V_{-sat} = -3.5\,\mathrm{V}$, and using $V_{eb} = 0.68\,\mathrm{V}$ and $V_{ebmx} = 0.70\,\mathrm{V}$ gives $V_{cth} = V_{th} + 8.8\,\mathrm{mV}$.

Figure 4 shows the measured approximation of the Hill inhibition for the single gene circuit of Figure 2 for $n = 3.2$, $\alpha = 218$, and $R_{hill} = 4\,\mathrm{k}\Omega$. The dots are the normalized output voltage V_i/V_{th} as a function of normalized input voltage V_{i-1}/V_{th}. It is apparent that as the input voltage surpasses V_{th} (at $x = 1$) the transistor current shuts off, closely following the numerically plotted Hill function (solid line). The location (at $x = 1$) and slope of the drop are set by equations (9) and (10), but the positive curvature decay to zero is controlled by R_{hill} in Figure 2. The value of R_{hill} is varied to match the transistor current's decay to that of the Hill function. Our previous circuit model for a single gene [10] used a piecewise-linear approximation to the Hill function and therefore did not include a positive curvature decay to zero.

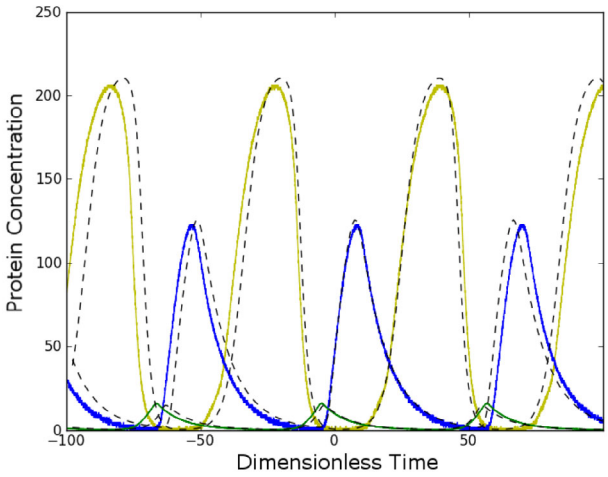

Fig. 5. Time series showing Repressilator protein concentrations A (large amplitude), B (mid amplitude), and C (small amplitude). Numerical (dashed) and circuit measurements (continuous lines) for Repressillator with no quorum sensing ($\kappa = 0$ in Eq. (1)); $n = 3.2, \alpha = 218$, $\beta_1 = 0.5, \beta_2 = \beta_3 = 0.1, R_{hill} = 4\,\mathrm{k}\Omega$.

The assumption that the output of op-amp U2 is saturated at V_{-sat} when $V_{i-1} = 0$ (no inhibition) means that $G_1 G_{-2} V_{cth} > -V_{-sat}$. Using the relations between V_{cth} and V_{th} (Eq. (10)), between V_{th} and α (Eq. (4)), and between $G_1 G_{-2}$ and $n\alpha$ (Eq. (9)), we find the restriction on the Hill coefficient

$$n > \frac{2\left(s(5 - V_{-sat}) - 2V_{be} + V_{bemx}\right)}{s(5 - V_{-sat}) - V_{bemx}}. \tag{11}$$

For our circuit values this gives a minimum Hill coefficient of $n = 2.12$. This restriction is generally not a problem since the Repressilator in equation (1) has a stable fixed point for $\kappa = 0$, and therefore is not an oscillator for $n < 2$ over a wide range of α and identical β.

The Repressilator consisting of the 3-gene ring in Figure 1 is modeled by connecting three single-gene circuits in a closed loop depicted by the 3 gene-triangles (A,B,C) in Figure 3. Figure 5 shows the measured time series and simulations (dashed lines) for a Repressilator demonstrating the stable protein oscillations (A, B, C) with different amplitudes that occur for different protein time-scales $\beta_1 = 0.5$, $\beta_2 = 0.1$, and $\beta_3 = 0.1$.

2.2 Circuit for Repressilator with quorum sensing

The circuit for a Repressilator with QS feedback shown in Figure 3 is a complete redesign of that presented previously [11]. The feedback from B through the current source $I(B)$ to S_1, then through $I(S)$ to C corresponds to the AI feedback loop between B and c in Figure 1. We analyse the circuit to derive relations between the mathematical model and circuit values. Figures 6 and 7 show the circuits for the voltage dependent current sources $I(B)$ and $I(S)$ used in Figure 3.

The circuit equation corresponding to equation (1d) comes from circuit analysis for the voltage representing S_1 across the capacitor C_S in Figure 3

$$R_S C_S \frac{dV_{S1}}{dt} = -V_{S1} + R_S I(B) - \frac{R_S}{R_d}\left(V_{S1} - V_{ext}\right). \tag{12}$$

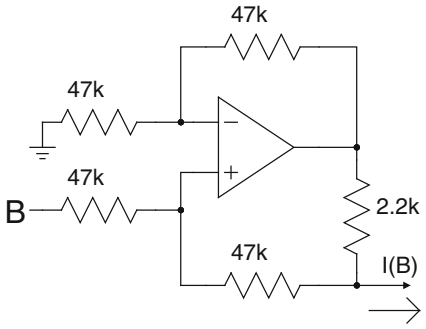

Fig. 6. Voltage controlled current source $I(B)$. Protein B voltage controls the current source to the S-voltage. $I(B) = V_B/(2.2\,\mathrm{k}\Omega)$. Op-amp has low offset voltage (below 0.5 mV).

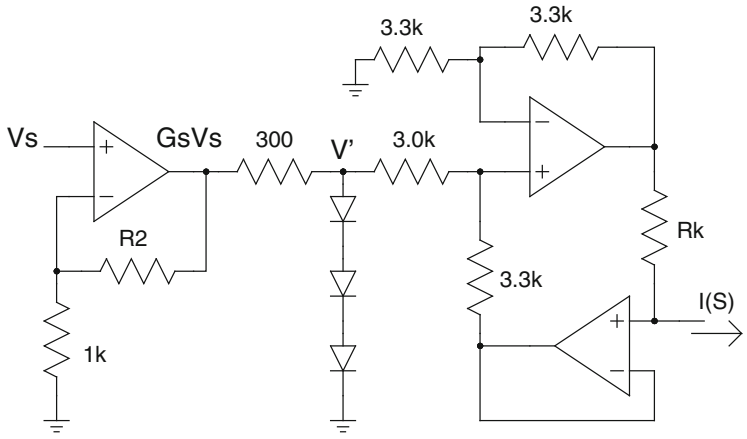

Fig. 7. Voltage controlled current source $I(S)$. Auto-inducer S-voltage V_S controls the current source feeding back to protein C-voltage. For small S the diodes are not conducting and $I(S) = G_S V_S/R_k$. For large S the diodes are forward biased and the voltage V' remains close to 2 V causing the output $I(S)$ to level off. Diodes are 1N4148. Op-amps (LF412) have low offset voltage (below 0.5 mV).

V_{S1} and V_{ext} correspond to the scaled voltages S_1 and S_{ext} in Figure 3. Multiplying both sides by k_{S0}, setting $k_{S0}R_SC_S$ to be the same as the time-scale R_CC_0 defined for the single-gene circuit, using $I(B) = V_B/2.2\,\mathrm{k}\Omega$ from Figure 6, $V_B = V_{th}B$, and dividing by a scaling factor V_{sth} gives

$$\frac{dS_1}{dt} = -k_{S0}S_1 + k_{S0}\frac{R_S}{(2.2\,k\Omega)}\frac{V_{th}}{V_{sth}}B - k_{S0}\frac{R_S}{R_d}(S_1 - S_{ext}) \tag{13}$$

where $V_S = V_{sth}S$ and $V_{ext} = V_{sth}S_{ext}$. Comparison with equation (1d) gives relations for the activation rate k_{S1} of auto-inducer and the membrane diffusion parameter η.

$$k_{S1} = k_{S0}\frac{R_SV_{th}}{(2.2\,k\Omega)V_{sth}}, \quad \eta = k_{S0}\frac{R_S}{R_d}. \tag{14}$$

Equation (14) sets the scaling factor V_{sth}.

The equation for the protein C voltage is found in the same way as equation (3) with the addition of the current $I(S)$ from the feedback loop in Figure 3.

$$R_CC_0\frac{dC}{dt} = \frac{C_0}{C_3}\left(-C + \frac{I_tR_C}{V_{th}} + \frac{I(S)R_C}{V_{th}}\right). \tag{15}$$

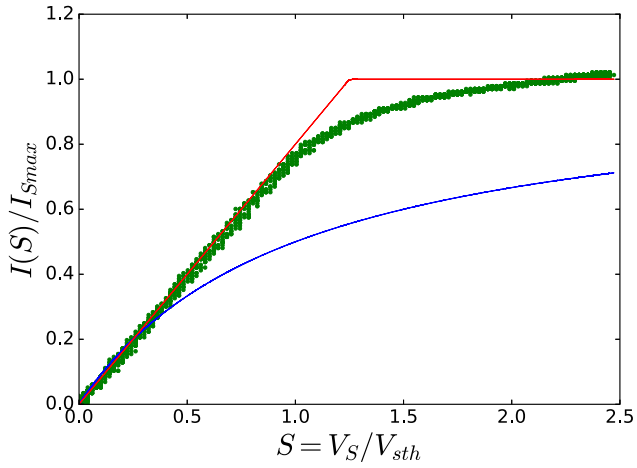

Fig. 8. Measured normalized AI activated current(dots) and models; piece-wise-linear $\min(0.8S, 1)$ (upper line) and hyperbola $S/(1+S)$ (lower line). For $\kappa = 21, \alpha = 135$. Reproduced from reference [17].

Comparison with equation (2) shows that

$$\frac{I(S)R_C}{V_{th}} = \kappa \ \min(0.8S, 1) \tag{16}$$

Equation (16) imposes two constraints. First, the maximum value of $I(S)$ must correspond to the right-hand-side maximum κ occurring for $S \geq 1.25$, giving

$$I(S \geq 1.25) \equiv I_{Smax} = \frac{\kappa V_{th}}{R_C}. \tag{17}$$

The maximum current is implemented by adjusting the gain G_S in Figure 7 so that the $S = 1.25$ input voltage $V_S = 1.25V_{sth}$ creates a current of 1 mA in the series diodes causing $V' = 3 \times 0.63 = 1.9\,\mathrm{V}$. The required op-amp output is $G_S(1.25)V_{sth} \approx 1.9 + (1\,\mathrm{mA})(300\,\Omega) = 2.2\,\mathrm{V}$ which provides the appropriate value for G_S. Secondly, for currents below the maximum value, equation (16)'s slopes must be the same. From Figure 7 the current source is $I(S) = G_S V_S/R_\kappa$. For currents below I_{Smax} we use equation (16) and the relation for V_{sth} in equation (14) to find the relation between model parameter κ and circuit value R_κ,

$$R_\kappa = k_{s0}\frac{G_S R_C R_S}{0.8(2.2\,\mathrm{k}\Omega)k_{s1}\kappa}. \tag{18}$$

All the values on the right-hand-side except κ have been previously determined, therefore equation (18) provides a direct link between parameter κ and circuit value R_κ. For the values used here the result is $R_\kappa = (56.8G_S)/\kappa$ in kΩ.

Figure 8 shows the measured normalized current $I(S)/I_{Smax}$ from the circuit in Figure 7, the piece-wise-linear model $\min(0.8S, 1)$ (used in Eq. (2)), and the hyperbola $S/(1+S)$ (Eq. (1c)) for $\kappa = 21.3$, $V_{th} = 0.0219\,\mathrm{V}$, and gain $G_s = 1.76$. The piece-wise-linear function intersects the hyperbola at $S = 0$ and 0.25.

We now consider the circuit which creates the AI concentration in the external medium S_{ext}. Each Repressilator circuit contributes its intracellular AI concentration S_i to the external concentration S_{ext}. Figure 3 shows how two Repressilators are

coupled by concentrations S_1 and S_2 combining to produce

$$S_{ext} = \frac{2R_Q}{4.7\,\mathrm{k}} S_{ave} = QS_{ave} \tag{19}$$

where $S_{ave} = (S_1 + S_2)/2$. $Q = 2R_Q/4.7\,\mathrm{k\Omega}$ is a dilution factor which in a biological setting ranges from 0 to 1. For purposes of exploring dynamics in the full parameter range of the mathematical system, we use a $5\,\mathrm{k\Omega}$ potentiometer for R_Q so that we can vary Q from 0 to 2. Our previous circuit design [11] limited Q variation from 0 to 1.

2.3 Selection of circuit values

Here we summarize the practical results for choosing circuit values in Figures 2 and 3. The model parameters are n, α, $\beta's$, κ, k_{s1}, and η. Some circuit values are chosen independent of the model parameters. We choose $R_C = R_S = 1\,\mathrm{k\Omega}$ and $C_0 = C_S = 0.1\,\mu f$ for characteristic time 0.10 ms, $R_E = 222\,\Omega$, $V_{-sat} = -3.5\,\mathrm{V}$ (for the LF412 op-amp powered by $\pm 5\,\mathrm{V}$), and the voltage divider fraction (R_{b1} and R_{b2}) in Figure 2 as $s = 420/2620 = 0.160$. Resulting measured quantities for the transistor are $I_{max} = 2.95\,\mathrm{mA}$ at $V_{ebmx} = 0.70\,\mathrm{V}$, and $1.5\,\mathrm{mA}$ at $V_{eb} = 0.68\,\mathrm{V}$. These currents were shown to be consistent with predictions using the standard large-signal transistor model $I(V_{eb}) = I_S \exp(V_{eb}/V_T)$.

For Figure 2, equation (4) gives V_{th} and C_i, equation (9) gives overall gain $G_1 G_{-2}$, and equation (10) gives V_{cth}. For Figure 3, equation (18) gives R_κ, op-amp gain $G_S = 0.8 \times 2.2\,\mathrm{V}/V_{sth}$, where V_{sth} is given by equation (14). The only circuit value not determined by the model parameters is R_{hill} in Figure 2. It is convenient to incorporate trim-pots into R_{hill} to adjust the Hill function's positive curvature decay to zero.

For many choices of parameters the AI concentration S stays below 1, in which case the S activation term $\min(0.8S, 1) \to 0.8S$ meaning there is no need to amplify V_S to impose saturation of $I(S)$. Thus, the current source $I(S)$ in Figure 7 can be simplified by leaving out the non-inverting op-amp at the input and the 3 diodes, so that V_S connects directly to the $300 + 3k = 3.3\,k\Omega$. In this case $G_S = 1$ in equation (18).

2.4 Setting initial conditions

The ability to set initial conditions is crucial when studying systems with multistability so that all attractors can be captured. We use the 4066 quad analog switch to impose initial conditions by momentarily connecting "protein" capacitor voltages to desired initial values set by trim-pot voltage dividers with op-amp followers. The 4066 is gated by the output of a 555 timer controlled by a push-button momentary switch (circuit not shown). Improved performance of the 4066 switch is achieved by powering it with 0 and $+15\,\mathrm{V}$, compared to the synthetic genetic network circuits powered by $\pm 5\,\mathrm{V}$.

2.5 Other design considerations

The inexpensive 2N3906 *pnp* transistors used in the gene circuits were selected from a large batch to have nearly the same saturation current, $I_S = 7 \pm 1$ fA, by performing in-house measurements.

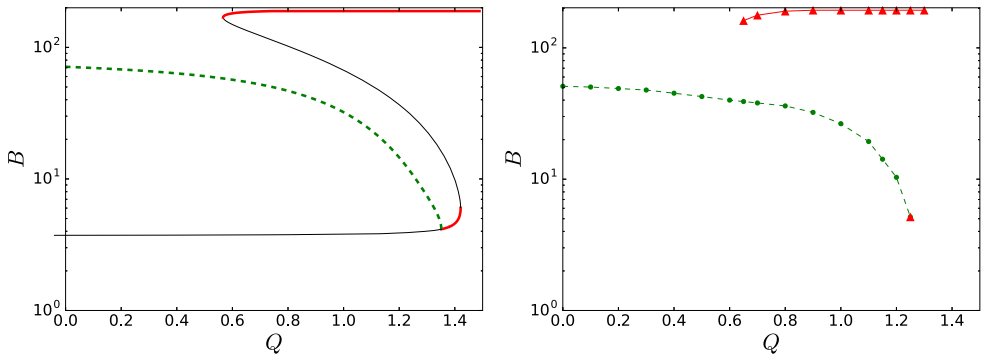

(a) Numerical (b) Measured

Fig. 9. Numerical and measured Q-continuation bifurcation diagrams showing amplitude of protein B for a single Repressilator with quorum sensing. (a) Numerical: stable (thick solid line) and unstable (thin solid) steady-state. Stable limit cycle (thick dashed). (b) Measured: data points for stable steady-state (triangles) and stable limit cycle (circles).

For the case of coupled Repressilator circuits, care was taken to distribute the $\pm 5\,\mathrm{V}$ power rails and ground paths symmetrically to both Repressilators. The measured voltage difference during operation between respective rails and respective grounds of the two Repressilators was less than $1\,\mathrm{mV}$.

3 Measurments: quorum sensing circuit

We now present experimental results incorporating the new QS circuitry. We begin with a single Repressilator with QS feedback, followed by two coupled Repressilators.

The case of a single Repressilator with QS feedback corresponds to setting $S_{ext} = Q \times S$ in equation (1d). Measured results from the QS circuit are compared to predictions from numerical simulations using the XPPAUT software [21]. The desired goal is that the circuit and the simulations have the same structure of dynamical behaviors. A convenient way to do this dynamical comparison is to compare their Q-continuation bifurcation diagrams shown in Figure 9. These diagrams show the possible amplitudes of protein B for different Q-values. Figure 9a shows numerical stable (thick line) and unstable (thin) steady-states (SS), and stable limit cycle (LC) oscillations (dashed). Figure 9b shows data points for stable SS (triangles) and stable LC (circles). The B-values for the circuit were obtained by normalizing the measured voltage amplitudes by $V_{th} = 15.5\,\mathrm{mV}$ which corresponds to the parameter values used in the simulation; $n = 3.0$, $\alpha = 190$, $\beta_i = 0.5, 0.1, 0.1$, and $\kappa = 10$. $R_{hill} = 2.7\,\mathrm{k\Omega}$.

In both simulation and circuit measurements Figure 9 shows that increasing Q causes the LC to decrease in amplitude until reaching the low-B-SS, and there is coexistence of high-B-SS and LC over a broad range of Q-values from approximately 0.6 to 1.3. Both bifurcation diagrams predict that decreasing Q will cause a transition to LC for a system starting from the high-B-SS. Figure 10 shows an oscilloscope screenshot of this Q-induced high-B-SS to LC transition when Q was slowly decreased by adjusting trim-pot R_Q in Figure 3. The transition occurred at a value of $1.5\,\mathrm{k\Omega}$ corresponding to $Q = 2 \times 1.5/4.7 = 0.64$ agreeing well with the left-side endpoint of the high-B-SS in the bifurcation diagrams.

The agreement between the circuit and simulation results is not exact in Figure 9, however, the qualitative structure and relative location of dynamical behaviors are

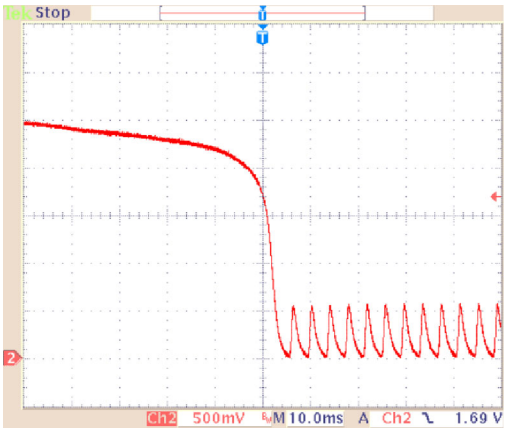

Fig. 10. Screenshot (oscilloscope) of high-B-SS to LC transition caused by decreasing Q at 0.64 for a single Repressilator circuit with QS feedback. Protein B voltage shown. Parameters: $n = 3$, $\alpha = 190$, $\kappa = 10$, $R_{hill} = 2.7$ kΩ.

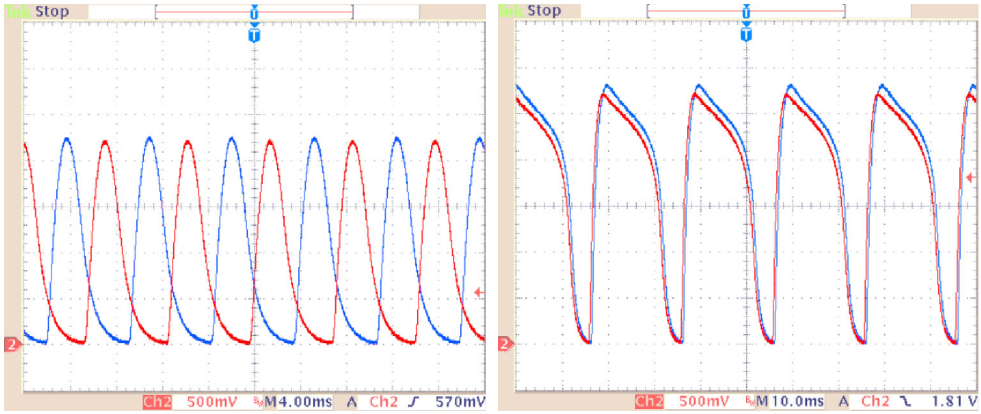

(a) Anti-phase (b) In-phase

Fig. 11. Screenshots of anti-phase and in-phase limit cycles for two QS-coupled Repressilator circuits. The protein B voltages from each Repressilator circuit are shown. Both screenshots use the same circuit values, thus demonstrating the coexistence of AP and IP limit cycles.

the same. For the circuit the low-B-SS was stable over a Q-range narrower than the resolution of Q-values and therefore appears as the single triangle data point at the end of the LC-branch. We note that the simulations are able to find the unstable SS (thin lines in Fig. 9a), whereas the circuit, of course, only finds stable dynamics. We conclude that the quorum sensing circuit achieves the goal of having the same dynamical behavior as the mathematical model.

The motivation for the circuit improvements presented here is to extend our previous investigations to coupled Repressilators. Figure 11 shows examples of the homogeneous limit cycles for two coupled Repressilators. The screen-shots show the B-protein voltages of the two Repressilator circuits. The "repressive" coupling scheme in equations (1) produces a multistable system whose stable oscillations are predominantly anti-phase (AP) [16] like those in Figure 11a. Interestingly, under appropriate parameter values it is possible to find stable in-phase limit cycles (IP)

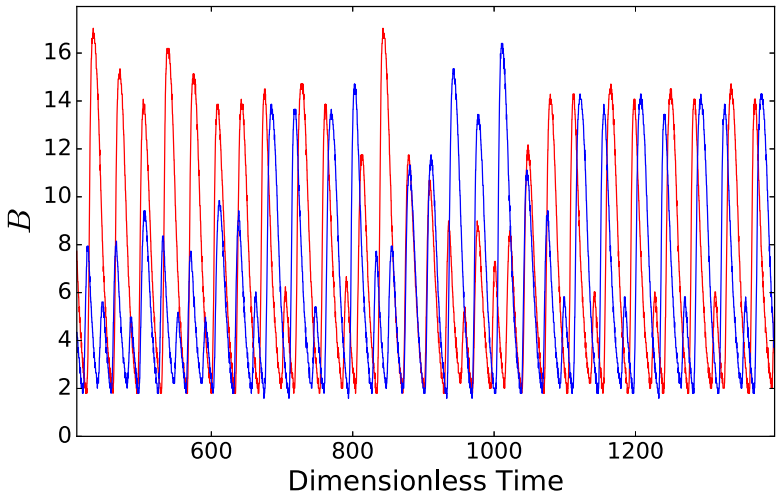

Fig. 12. B-voltages measured from circuit model of two QS-coupled Repressilators exhibiting complex dynamics containing transient pieces of asymmetric period-1:2 and symmetric period-3 limit cycles. $n = 3.2, \alpha = 148$.

like those in Figure 11b, which coexist with AP. Both screen-shots use the same parameters ($n = 4$, $\alpha = 143$, $\beta_i = 0.5, 0.1, 0.1$, $\kappa = 4.8$, $R_{hill} = 9$ kΩ) and both the AP and IP can be accessed simply by smoothly varying the coupling strength Q. AP is the sole stable state at small Q and as Q is increased the amplitude of the AP decreases until the AP becomes unstable and transitions to a stable steady-state characterized by both B-proteins being at the high value. When Q is then decreased there is a transition to IP at the endpoint of the stable steady-state (similar to the transition induced by decreasing Q for the single Repressilator in Fig. 10).

A rich variety of complex dynamics occurs for Hill coefficients $n = 3.0$ to 3.2 as described in reference [17]. Here we show results from the improved circuit demonstrating how symmetric and asymmetric high period limit cycles influence the complex dynamics in the regime where the AP limit cycle is unstable. Figure 12 shows complex dynamics containing transient durations of high period oscillations–symmetric period-3 and asymmetric period-1:2 limit cycles. The evolution of complex behavior as Q is varied may be seen in the "sequential period maps" $T(n+1)$ versus $T(n)$ where $T(n)$ are the return times (subperiods) for a given Poincaré section. Figure 13 shows measured sequential period maps from circuits with various Q-values. Figure 13a is for an asymmetric-4:4 limit cycle which is stable because the symbols (+ and o) for the two B-proteins do not mix. Figure 13b is from a stable 3:3 limit cycle which is symmetric thereby requiring the symbols to mix. Figure 13c is from an unstable asymmetric-1:2 limit cycle in which the two B-proteins are "switching roles" causing mixing. Figure 13d is from a complex time series, a portion of which is shown in Figure 12, which contains pieces of the asymmetric-1:2 and the symmetric-3:3 limit cycles. It is apparent that the locust of points in (d) has contributions from (b) and (c).

4 Incorporation of additive noise

Additive noise may be included using a simple noise circuit shown in Figure 14 based on the breakdown of a reverse biased base-emitter junction as described previously [12]. Noise is added to a protein by disconnecting its R_C from ground in Figure 2 and connecting it to the noise circuit output as shown in Figure 14. The

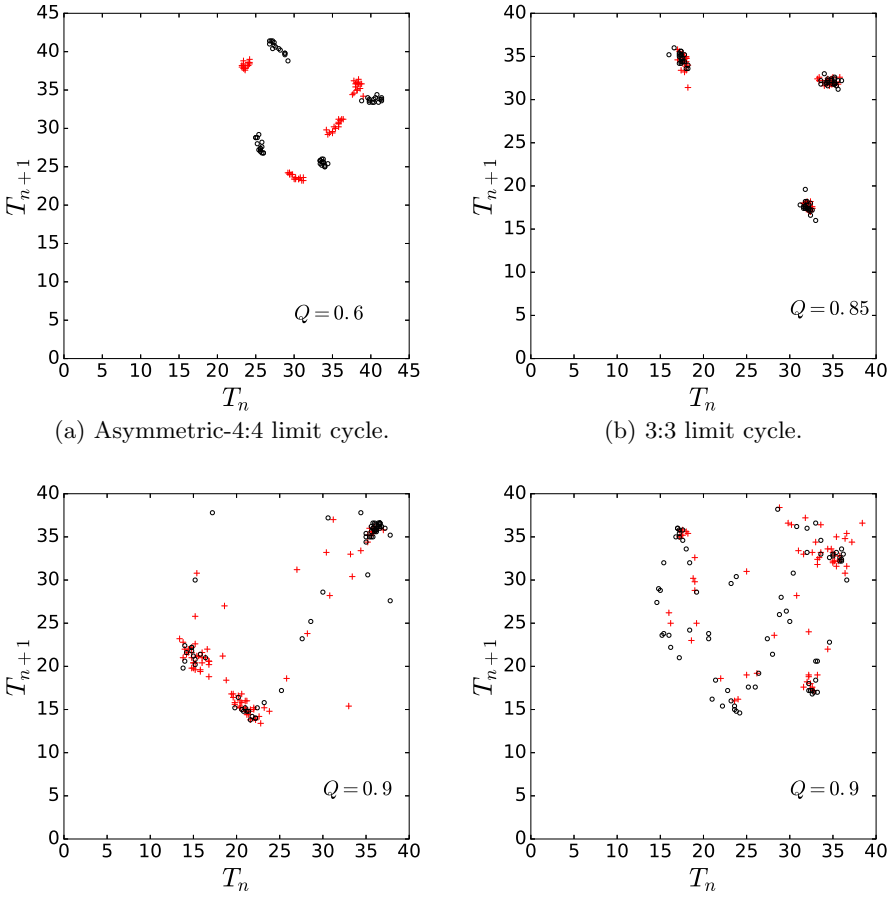

(a) Asymmetric-4:4 limit cycle. (b) 3:3 limit cycle.

(c) Unstable asymmetric-1:2 limit cycle. (d) Unstable with pieces of As-1:2 and 3:3.

Fig. 13. Sequential period maps constructed from time-series circuit measurements for various Q within the unstable AP regime. Return times for the two B proteins indicated by $+$ and o. Q-values for (c) and (d) are within the experimental resolution of 0.9.

potentiometer at the second op-amp adjusts the noise amplitude. Using the same procedure used to find equation (3), the equation for the gene's protein voltage V_i is easily found to be

$$(1\,\mathrm{k\Omega})C_i\frac{dV_i}{dt} = V_i - V_{noise} + (1\,\mathrm{k\Omega})I_t. \tag{20}$$

The noise is symmetric about zero and therefore the minus sign is irrelevant, thus accomplishing the task of adding noise to the protein voltage V_i.

Comparison of the noise-influenced dynamical results from circuit measurements and numerical predictions requires careful connection of the electronically generated noise characteristics to the simulated noise. Here we summarize those connections, which were derived previously [12]. In simulations additive noise is typically represented by $D\eta(t)$ where $\eta(t)$ is a zero-mean Gaussian noise with unit variance and the amplitude D is the noise strength. The electronically generated noise is characterized by its rms amplitude V_{Nrms} and its frequency bandwidth f_c. The relation between

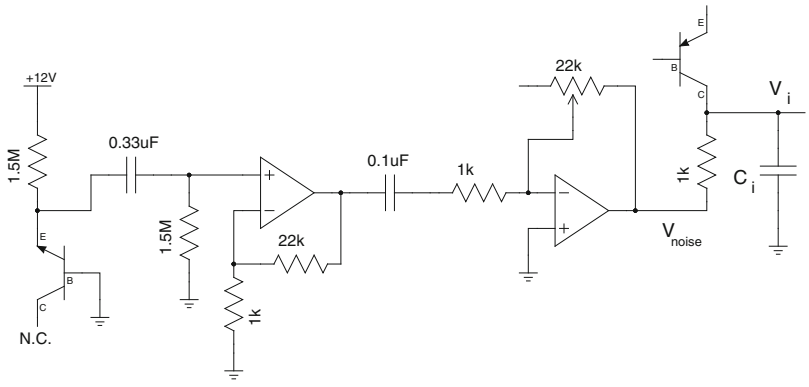

Fig. 14. Noise circuit. 2N3904 *npn* on left has no connection at its collector. 2N3906 *pnp* on right is from the gene circuit (Fig. 2). Op-amps are OPA228 powered by ±12 V. Noise is produced by stochastic breakdown of the reverse biased base-emitter *pn* junction of the transistor on the left and amplified by two stages of op-amps producing $V_{\rm noise}$ which is connected to the 1 kΩ resistor of the gene circuit.

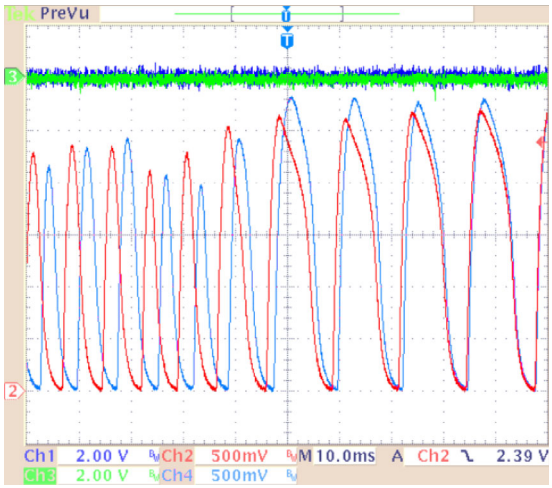

Fig. 15. Screen-shot of noise-induced transition from anti-phase (AP) to in-phase (IP) oscillation for two QS-coupled Repressilator circuits. Independent noise (top two traces) was added to each B-protein voltage.

the simulated noise strength D and the measured strength V_{Nrms} is [12]

$$D = \frac{V_{Nrms}}{V_{th}\sqrt{\gamma(RC)f_c}} \tag{21}$$

where RC is the characteristic time of the Repressilator, and $\pi/4 \leq \gamma \leq \pi/2$ depending on the gain of the second amplifier in Figure 14. The noise bandwidth is determined by the op-amp's gain-bandwidth product (33 MHz for the OPA228) and the gain of the non-inverting amplifier in Figure 14 (about 20×) resulting in a noise bandwidth of $f_c = 33/20 \approx 1.5$ MHz.

As a demonstration, we add independent noises to each B-protein for the case of coexistence of AP and IP states used for Figure 11 ($n = 4$, $\alpha = 143$, $\kappa = 4.8$). Multiple

transitions between the states were observed. Figure 15 shows a noise-induced transition from AP to IP. The top two traces are the added noises with rms-amplitudes of $V_{Nrms} = 0.156\,\mathrm{V}$. Equation (21) gives the corresponding noise strength for simulation $D \approx 0.6$, found using $\alpha = 143$ and $I_{max}R_C = 2.95\,\mathrm{V}$ to give $V_{th} = 20.6\,\mathrm{mV}$, characteristic time $RC = 0.1$ ms, and taking $\gamma = 1$.

5 Conclusion

We presented a revised design for our electronic circuit model of a synthetic genetic network comprised of Repressilators coupled together by quorum sensing. Two significant improvements over previous versions [10,11] were shown: The incorporation of the large-signal transistor model into the derivation of the circuit's Hill function repression yields improved connections between mathematical parameters and circuit values, and a complete redesign of the quorum sensing circuitry produced superior modeling of the quorum sensing activation and allowed expansion of the quorum sensing circuit's parameter range to match that of the mathematical model. In addition, we describe how to set initial conditions, a feature crucial to investigating multistability. Circuit behavior was verified by comparing bifurcation diagrams obtained from measurements and numerical simulation. These circuit revisions were important because they allow us to extend previous investigations to the case of two coupled Repressilators. Here we demonstrated the coexistence of IP and AP limit cycles, noise-induced transitions between these states, and the influence of high period limit cycles on the complex dynamics. Recently, the improved circuit was used to find a rich dynamical landscape, including many regimes of multistablilty of a variety of dynamical states, and a broad regime of unstable AP limit cycle which contains an interesting evolution of complex behavior including symmetric and asymmetric chaos [17].

S.K.D. acknowledges support by the University Grants Commission (India) Emeritus Fellowship. The authors thank Evgeny Volkov for valuable contributions.

References

1. J. Hasty, F. Isaacs, M. Dolnik, D. McMillen, J.J. Collins, Chaos: An Interdiscip. J. Nonlinear Sci. **11**, 207 (2001)
2. M. Elowitz, W.A. Lim, Nature **468**, 889 (2010)
3. Y. Benenson, Nat. Rev. Genet. **13**, 455 (2012)
4. T.S. Gardner, C.R. Cantor, J.J. Collins, Nature **403**, 339 (2000)
5. M.B. Elowitz, S. Leibler, Nature **403**, 335 (2000)
6. J. Mason, P.S. Linsay, J.J. Collins, L. Glass, Chaos: An Interdiscip. J. Nonlinear Sci. **14**, 707 (2004)
7. A. Wagemakers, J.M. Buldú, J. García-Ojalvo, M.A.F. Sanjuán, Chaos: An Interdiscip. J. Nonlinear Sci. **16**, 013127 (2006)
8. J.M. Buldú, J. García-Ojalvo, A. Wagemakers, M.A.F. Sanjuán, Int. J. Bifurc. Chaos **17**, 3507 (2007)
9. I.T. Tokuda, A. Wagemakers, M.A.F. Sanjuán, Int. J. Bifurc. Chaos **20**, 1751 (2010)
10. E.H. Hellen, E. Volkov, J. Kurths, S.K. Dana, PLoS ONE **6**, e23286 (2011)
11. E.H. Hellen, S.K. Dana, B. Zhurov, E. Volkov, PLoS ONE **8**, e62997 (2013)
12. E.H. Hellen, S.K. Dana, J. Kurths, E. Kehler, S. Sinha, PLoS ONE **8**, e76032 (2013)
13. J. García-Ojalvo, M.B. Elowitz, S.H. Strogatz, PNAS **101**, 10955 (2004)
14. I. Potapov, B. Zhurov, E. Volkov, Chaos: An Interdiscip. J. Nonlinear Sci. **22**, 023117 (2012)
15. E. Ullner, A. Zaikin, E. I. Volkov, J. García-Ojalvo, Phys. Rev. Lett. **99**, 148103 (2007)

16. E. Ullner, A. Koseska, J. Kurths, E. Volkov, H. Kantz, J. García-Ojalvo, Phys. Rev. E **78**, 031904 (2008)
17. E.H. Hellen, E. Volkov, Phys. Rev. E **95**, 022408 (2017)
18. S.H. Strogatz, I. Stewart, Sci. Am. **269**, 102 (1993)
19. C.M. Waters, B.L. Bassler, Annu. Rev. Cell Dev. Biol. **21**, 319 (2005)
20. I. Potapov, E. Volkov, A. Kuznetsov, Phys. Rev. E **83**, 031901 (2011)
21. B. Ermentrout, *Simulating, Analyzing, and Animating Dynamical Systems: A Guide to XPPAUT for Researchers and Students* (SIAM, 2002)